[Frontiers in Bioscience E4, 1081-1096, January 1, 2012]

Functional oncoimaging techniques with potential clinical applications

Thomas C. Kwee[1], Sandip Basu[2], Babak Saboury[3], Abass Alavi[3], Drew A. Torigian[3]

[1]Department of Radiology, University Medical Center Utrecht, Utrecht, The Netherlands, [2]Radiation Medicine Centre (BARC), Tata Memorial Hospital Annexe, Parel, Bombay 400012, India, [3]Department of Radiology,University of Pennsylvania School of Medicine, Hospital of the University of Pennsylvania, Philadelphia, PA

TABLE OF CONTENTS

1. Abstract
2. Introduction
3. Functional Imaging of Tumor Physiology
- *3.1. Perfusion imaging*
- *3.2. Diffusion imaging*
- *3.3. Elastography*
- *3.4. Functional lymph node imaging*

4. Functional Imaging of Tumor Molecular Processes
- *4.1. Metabolic imaging*
  - *4.1.1. Glucose metabolism*
  - *4.1.2. Amino acid metabolism*
- *4.2. Cell proliferation imaging*
- *4.3. Oxygenation imaging*
- *4.4. Molecular imaging with targeted imaging agents*
  - *4.4.1. Somatostatin receptor imaging*
  - *4.4.2. Estrogen receptor imaging*
- *4.5. Angiogenesis imaging*
- *4.6. Apoptosis imaging*
- *4.7. Magnetic resonance spectroscopy*

5. Conclusion
6. Acknowledgement
7. References

1. ABSTRACT

Structural imaging is currently used in standard clinical practice on a daily basis to qualitatively or semiquantitatively detect, characterize stage, assess post-therapeutic change in, and determine recurrence of malignant tumors based on structural features or gross degree of contrast enhancement. Unfortunately, structural imaging does not provide information about tumor physiology, biological processes, and molecular features, and as such tumors cannot be fully characterized and monitored. In order to improve the evaluation of tumors and to reduce cancer-related morbidity and mortality, there is a need for functional imaging modalities which allow visualization and quantification of physiological and biochemical processes *in vivo*. This article will review a selection of the wide variety of functional imaging methods available for non-invasive evaluation of tumor physiology and molecular processes.

2. INTRODUCTION

Cancer is a major public health problem in the United States and many other parts of the world. Currently, 1 in 4 deaths in the United States is due to cancer (1). Imaging plays a crucial role in oncology, and is being used for screening, diagnosis and staging, prognosis assessment, image-guided treatment, treatment response assessment, and detection of tumor recurrence. As such, imaging may reduce cancer incidence and mortality and improve survival. Imaging technologies used to assess patients with cancer may be grossly subdivided into structural and functional imaging categories. Structural imaging entails the assessment of morphologic features or gross degree of contrast enhancement of normal tissues/organs of the body and of malignant lesions within these structures. Computed tomography (CT), magnetic resonance imaging (MRI), and ultrasonography (US) are the prototypical imaging technologies that are currently used to perform structural imaging in oncology (2-4). However, functional or

metabolic changes at the molecular, subcellular, or cellular level may occur well before gross structural or contrast enhancement changes become visible (5). Furthermore, macroscopic abnormalities are nonspecific and often seen in non-neoplastic conditions. In addition, data regarding physiology, biological processes, and molecular characteristics of tumors are not available by structural-based imaging.

Thus, structural imaging lacks the desired information to fully characterize or monitor lesions. In order to improve the evaluation of tumors, there is a need for functional imaging modalities which allow visualization and quantification of physiological and biochemical processes *in vivo*. The combination of structural and functional imaging is expected to improve the management of patients with cancer or those at risk for cancer (6). Functional imaging can be implemented through use of CT, MRI, and US, as well as through positron emission tomography (PET), single-photon emission computed tomography (SPECT), and optical imaging (OI). An explanation of the basic properties of these imaging modalities can be read elsewhere (2-4). Functional imaging modalities can grossly be divided into a group that allows for evaluation of tumor physiology and a group that allows for assessment of tumor molecular processes. Examples of physiologic abnormalities that can be visualized in tumors are perfusion and diffusion, which may provide information on tumor neovascularity and tumor cellularity, respectively. Well-known examples of molecular imaging are PET using the radiotracer 2-^{18}F-fluoro-2-deoxy-D-glucose (FDG) and magnetic resonance spectroscopy (MRS), which allow for assessment of tumor glucose metabolism and detection and quantification of endogenous molecular compounds, respectively. The number of molecular targets for imaging is virtually endless, and other examples of molecular imaging that are under active investigation (and in which PET has a major role) include imaging of amino acid metabolism, cell proliferation, oxygenation, somatostatin and estrogen receptor expression, angiogenesis, and apoptosis. This article will review a selection of the wide variety of imaging methods that is available for the non-invasive evaluation of tumor physiology and tumor molecular processes.

3. FUNCTIONAL IMAGING OF TUMOR PHYSIOLOGY

3.1. Perfusion imaging

Tumor angiogenesis is considered an essential process for the growth, proliferation, and metastasis of solid tumors (7). Perfusion imaging is a method that allows non-invasive assessment of functional aspects of tumor neovascularity *in vivo* (8-10). Of all imaging techniques capable of providing qualitative and quantitative data of tumor vascularity, perfusion CT and dynamic contrast-enhanced MRI (DCE-MRI) have been widely investigated because they offer several advantages. First, CT and MRI are widely used in routine oncologic imaging, and perfusion studies can be incorporated relatively easily with routine examinations. Second, both CT and MRI offer good anatomic detail, and reliable measurements can be obtained with good spatial resolution. Third, and most importantly, these measurements have been shown to correlate with histologic markers of angiogenesis (8-10).

Perfusion CT and DCE-MRI are performed by obtaining sequential images before, during, and following the injection of a contrast agent (i.e. an iodine-based contrast agent for perfusion CT and (most frequently) a small molecular weight gadolinium-containing compound for DCE-MRI) (8-10). The relation between contrast concentration and enhancement is straightforward with CT; there is a direct linear relation between enhancement change and iodine concentration. As a result, the arterial input, which is required for quantitative analysis, can be measured directly from a conveniently placed artery. Thus, perfusion CT allows absolute quantification of perfusion in terms of blood flow, blood volume, mean transit time, and permeability (8). In contrast, the relation between MRI signal intensity change and the concentration of a paramagnetic contrast agent such as gadolinium is not so easily defined, because paramagnetic contrast agents indirectly induce signal intensity changes by affecting the relaxation properties of surrounding water protons. Therefore, quantification by DCE-MRI is technically more challenging. DCE-MRI can be performed using dynamic T2* methods or dynamic T1-weighted methods. Dynamic T2* methods employ the fact that the first pass of a contrast agent through a tissue causes a transient signal drop due to the local magnetic susceptibility (T2*) effects of the contrast agent. (Please note that T2*-weighting effects are due to a combination of T2-weighting effects and the effects of magnetic field inhomogeneity.) Dynamic T2* methods can provide information about (relative) tumor perfusion, which may pathologically be related to tumor grade and vessel density (8-10). Dynamic T1-weighted methods, on the other hand, employ the T1 shortening effects of the contrast agent that cause an increase in signal intensity as it passes from the blood into the extracellular space of tissues. Dynamic T1 methods can provide information about blood vessel permeability, capillary surface area, and leakage space, which may pathologically be related to tumor grade, microvessel density and levels of vascular endothelial growth factor expression (8-10). Perfusion CT (Figure 1) and DCE-MRI may be used for tumor detection, characterization, grading, and staging, determining prognosis, monitoring treatment, and detecting tumor relapse, as was shown in many types of cancer including brain, breast, prostate, cervix, liver, lung, and rectal cancer (8-10). Furthermore, these techniques may be used to measure the effects of (new) anti-angiogenic therapies (8-10). Greater detail about perfusion CT and DCE-MRI can be found elsewhere (8-10).

3.2. Diffusion imaging

Diffusion-weighted imaging (DWI) is an MRI method that allows non-invasive visualization and quantification of the random microscopic movement of water molecules (i.e. Brownian motion) within biologic tissues, without using any contrast agents (11). Pathologic processes that lead to changes in the diffusion of water molecules can be evaluated using DWI. For example, an increase in cellularity in tumors may lead to a decrease of

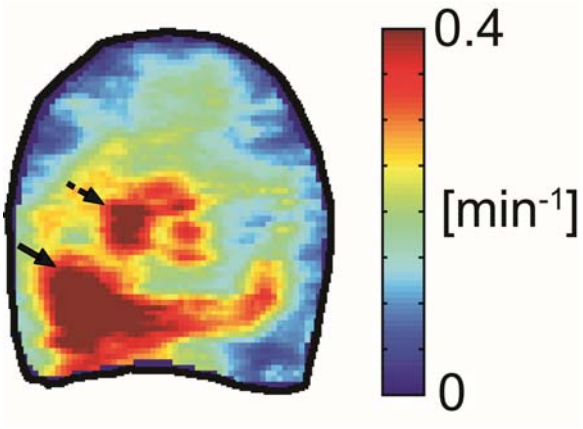

Figure 1. Perfusion CT imaging. Map of prostate gland K^{trans} (a measure of vascular permeability) from dynamic contrast-enhanced CT exam of a 64-year-old man, showing region with elevated K^{trans} values in peripheral zone, indicative for tumor. The high K^{trans} values in central gland could also reflect benign prostate hypertrophy. Images courtesy of Johannes G. Korporaal, PhD, University Medical Center Utrecht, Utrecht, The Netherlands.

the extracellular volume, where increased tortuosity of the extracellular space leads to reduced water mobility. On the other hand, necrosis and apoptotic processes may lead to loss of cell membrane integrity and decrease in cellularity. This, in turn, increases the amount of diffusion across the cell membrane and increases the proportion of water molecules in the extracellular space, where water mobility is less impeded (12-14). Currently, the most common application of DWI is in the diagnosis of acute ischemic stroke, a condition in which failure of the Na^+K^+ ATPase pump is believed to lead to a net displacement of water from the extracellular to the intracellular compartment, where water mobility is relatively more impeded (12). Thanks to technological advances, it has recently become possible to perform DWI outside the brain (13, 15), as a result of which the use of DWI in oncology is gaining widespread interest. Since DWI suppresses many unwanted signals from normal structures (e.g. signals of fat, muscles, vascular structures, cerebrospinal fluid, and gastrointestinal contents), lesions can be highlighted to better effect. As such, DWI may be a useful method for tumor detection and staging, and its comparison to FDG-PET/CT, a highly sensitive molecular imaging technique for detection and quantification of glucose uptake and retention within tumor sites which is often regarded as the most accurate non-invasive method for the evaluation of cancer, is of particular interest (Figure 2). (Please note that FDG-PET/CT will be described in further detail below under Metabolic Imaging.) For example, recent studies reported that the overall diagnostic performance of whole-body DWI (combined with conventional MRI sequences) was at least equal to that of FDG-PET for regional nodal (N) staging (16) and distant metastasis (M) staging (17, 18) in patients with non-small cell lung cancer.

Another important feature of DWI is that it allows for quantification of diffusion in biological tissue by means of so-called apparent diffusion coefficient (ADC) measurements, which may provide indirect information about tissue structure. ADC measurements may help in the characterization of tumors and in the early detection of response to therapy. For example, it has been reported that ADC measurements may facilitate grading of astrocytic brain tumors (19). Other studies (20, 21) showed that ADC measurements were at least equal to SUV measurements from FDG-PET in differentiating benign from malignant pulmonary lesions. Another recent study (22) reported that the preoperative maximum standardized uptake value (SUV) from FDG-PET, a semi-quantitative measure of lesional glucose uptake, and the ADC correlate with several prognostic factors, and that both indices may have the same potential for predicting the prognosis of breast cancer. Another promising application of DWI is in the early assessment of response to therapy. Recently, a voxel-based quantitative DWI approach was introduced (so-called parametric response mapping of diffusion (PRM_{ADC})), which allows visualization and calculation of spatial tumor diffusion coefficient changes during treatment (23, 24). PRM_{ADC} combined with traditional radiological response criteria 3 weeks after the start of radiation therapy proved to provide a significantly better prediction of response to therapy in patients with high-grade gliomas than traditional size criteria or PRM_{ADC} alone (24). The introduction of the PRM_{ADC} approach is a considerable step forward towards more individualized treatment planning, but its application outside the brain is technologically more challenging. Nevertheless, there are some studies which have already shown the feasibility of PRM_{ADC} as an early biomarker for the prediction of response to therapy in head and neck cancer (25), breast cancer (26), and bone marrow metastases from prostate cancer (27). Overall, DWI is a very promising method with many potential applications in oncological imaging. However, more research on DWI should be done before more definitive conclusions can be made regarding its exact value.

Interestingly, diffusion in the human body is not always isotropic. Particularly, it has been shown that diffusion is anisotropic in the nervous system. That is, diffusion is more impeded perpendicular to the course of the nerve fibers, while the highest diffusivity can be expected parallel to the course of the nerve fibers (28). The diffusion anisotropy of the nervous system can be exploited by performing diffusion tensor imaging (DTI). DTI is performed by applying diffusion-encoding gradients in 6 or more directions, and allows quantification and visualization of diffusion anisotropy (29). As such, it is possible to visualize the direction of cerebral white-matter tracts. DTI has been shown useful for pre-treatment assessment of white-matter tract involvement by tumor as well as for intraoperative visualization and localization of major white-matter tracts to decrease the chance of injury to normal tissues (30-32).

3.3. Elastography

Elastography involves imaging of the mechanical properties of tissue. Most elasticity imaging methods apply some kind of stress or mechanical excitation to the tissue, measure the tissue response to this stimulus, and from this

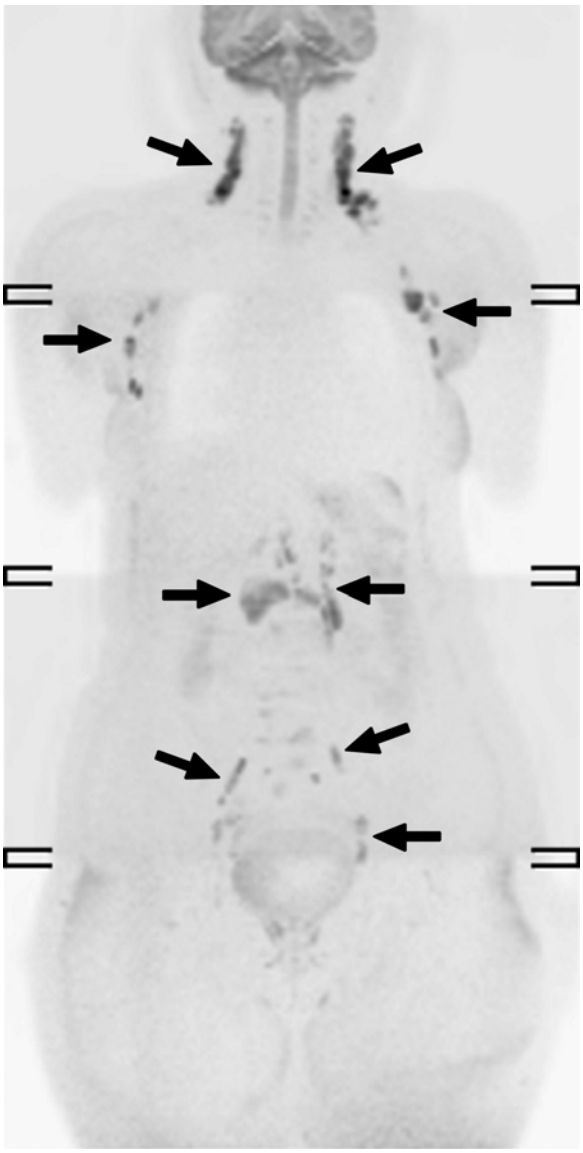

Figure 2. Diffusion imaging.Whole-body DWI in 67-year-old woman with small lymphocytic lymphoma. Coronal maximum intensity projection grey-scale inverted DWI shows supra- and infradiaphragmatic lymph node involvement (arrows), corresponding to Ann Arbor stage III. Image courtesy of Thomas C. Kwee, MD, University Medical Center Utrecht, Utrecht, The Netherlands.

response calculate parameters that reflect the mechanical properties (33). Cross-sectional imaging modalities that can be used for tissue response measurement include US and MRI. US-based elasticity imaging, however, is limited in that it requires a suitable acoustic window and has a limited depth for measurements because of the limited penetration of ultrasound waves in tissue (33).

In the mid 1990s, magnetic resonance elastography (MRE) was developed, which involves inducing harmonic vibrations of acoustic-range frequencies in tissue and imaging the propagation of these vibrations in the tissue to calculate quantitative values for tissue mechanical parameters (33, 34). MRE can be implemented on most modern MRI systems. Currently, the most important clinical application of MRE is the non-invasive assessment of hepatic fibrosis and cirrhosis, where the stiffness of the diseased liver is significantly higher than normal liver tissue stiffness (33, 35). However, the applications of MRE may also be extended to the characterization of tumors (Figure 3). For example, stiffness of malignant breast lesions is known to be higher than benign lesions and normal breast tissue (33, 36), which may be determined using MRE. Interestingly, a recent study in 39 and 29 benign breast lesions reported that MRE provided a significant diagnostic gain compared to dynamic contrast-enhanced MRI alone, with an increase of about 20% in specificity at 100% sensitivity (37). Oncological applications of MRE are very interesting, but more research is warranted before these can be implemented in routine clinical practice.

3.4. Functional lymph node imaging

The evaluation of lymph nodes plays a crucial role in the management of patients with cancer, because lymph node status has important therapeutic and prognostic implications. Current cross-sectional imaging modalities such as US, CT, and conventional MRI rely on insensitive and non-specific size criteria, and, therefore, lack the desired accuracy to characterize lymph nodes (38). Functional imaging techniques are under development to overcome these limitations.

Sentinel lymph node mapping is currently the most frequently employed method for functional lymph node imaging. The rationale for this method is that sentinel lymph nodes accurately reflect the status of the lymphatic basin draining a primary tumor. This assumption has been proven for malignant melanoma (39), early-stage breast cancer (40), and penile carcinoma (41). Sentinel lymph node mapping is usually performed with radiotracers (e.g. ^{99m}Tc-sulfur colloid, ^{99m}Tc-antimomy trisulfide colloid, or ^{99m}Tc-nanocolloid) and vital blue dyes. After intradermal injection around the tumor, the radioactive particles will become efficiently trapped in sentinel lymph nodes, whereas blue dyes typically pass into second echelon nodes. Subsequently, the sentinel lymph nodes can be identified by using pre-operative lymphoscintigraphy**,** an intraoperative gamma-detecting probe, and/or by the intraoperative visualization of blue-stained lymph nodes (42). Unfortunately, sentinel lymph node imaging does not allow for direct detection of involved lymph nodes, but directs surgical exploration to nodal sites that are potentially most vulnerable to cancer spread. Another drawback is the fact that only lymph nodes in the vicinity of the primary tumor can be assessed. Furthermore, increasing tumor growth in the sentinel lymph node may obstruct its afferent lymphatic vessels, as a result of which flow of lymph through the node may be diverted to the next draining lymph node, leading to lack of depiction of the originally involved sentinel lymph node (43-45). FDG-PET, which will be described in a later section, has an important advantage over sentinel lymph node mapping, in that it directly targets cancer cells in involved lymph nodes. Since

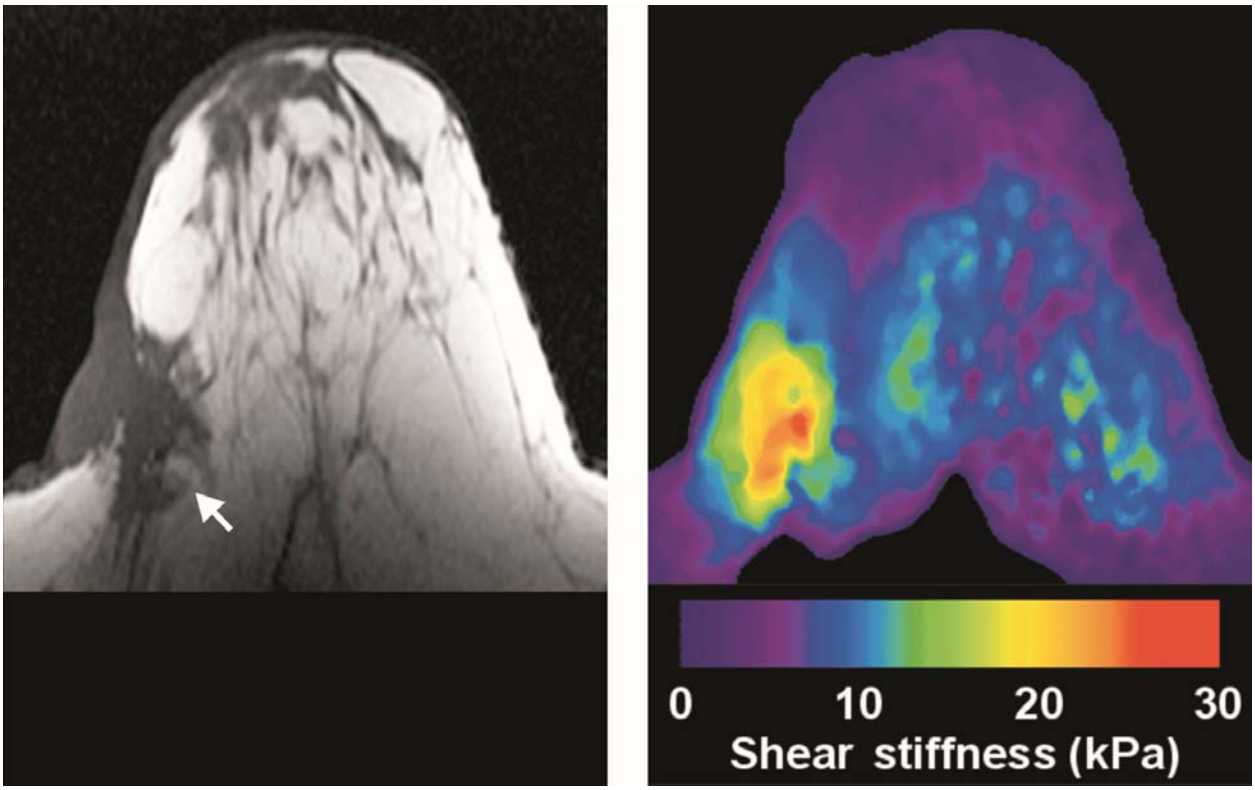

Figure 3. MR elastography imaging. MRE in 43-year-old woman with invasive ductal breast carcinoma in lateral breast. T1-weighted image (left) of breast shows irregular tumor mass (arrow), with thick overlying cutaneous tissue. MRE (right) shows focal area of high shear stiffness corresponding to location of known tumor mass. Reproduced with permission from (111).

systemically administered FDG arrives in the lymph node through its arterial blood supply, lymphatic obstruction and the subsequent reversal of lymph flow will not affect the performance of FDG-PET in diagnosing metastatic lymph nodes. Thus, in such settings, conventional sentinel lymph node imaging may be complementary with whole-body FDG-PET nodal imaging.

Yet another functional imaging technique that allows non-invasive detection of lymph node metastasis is ultrasmall superparamagnetic iron oxide (USPIO)-enhanced MRI (46). USPIO particles are nontargeted contrast agents that leak into the interstitium and reach the reticuloendothelial cells of lymph nodes via the lymphatic system, allowing for detection of micrometastases within normal-sized lymph nodes (Figure 4). The uptake of USPIO particles by normal lymph nodes creates local field inhomogeneities and turns them "black" (i.e. very low in signal intensity relative to that on precontrast images) on T2*-weighted images. Metastatic lymph nodes, on the other hand, lack uptake of USPIO particles and stay "white" (i.e. intermediate in signal intensity relative to that on precontrast images) on T2*-weighted images (46). A recent meta-analysis (47) including 38 studies that investigated the diagnostic performance of USPIO-enhanced MRI for nodal staging in various tumors reported that overall (lymph node-based) sensitivity and specificity of USPIO-enhanced MRI (88% and 96%, respectively) were higher than those of unenhanced MRI (63% and 93%, respectively). Although potentially useful, it should be realized that, unlike FDG-PET, USPIO-enhanced MRI indirectly reveals cancer sites in lymph nodes. Therefore, specificity of this method may be suboptimal in lymph nodes that are involved by non-neoplastic processes. Other important issues are that USPIO contrast agents have not yet been approved for human use either by the Food and Drug Administration (FDA) or by the European Medicines Agency (EMEA), and that the availability of these contrast agents is currently very limited. When USPIO contrast agents become more widely available, it would be of great interest for clinical studies to compare USPIO-enhanced MRI to FDG-PET for nodal staging.

DWI, which has been discussed previously, is another functional imaging technique that has been investigated for its use in lymph node characterization. Irrespective of their histological nature, lymph nodes can be identified as high signal intensity structures at DWI, because of their relatively long T2 relaxation time and impeded diffusivity. Assessment of signal intensity at DWI or quantification of diffusivity in lymph nodes by means of ADC measurements may aid in the histological characterization of lymph nodes, because different pathologic processes may lead to differences in diffusivity due to differences in cellularity, intracellular architecture, necrosis, and perfusion (14). Several studies reported the ADCs of metastatic lymph nodes to be significantly lower than those of non-metastatic lymph nodes, independent of

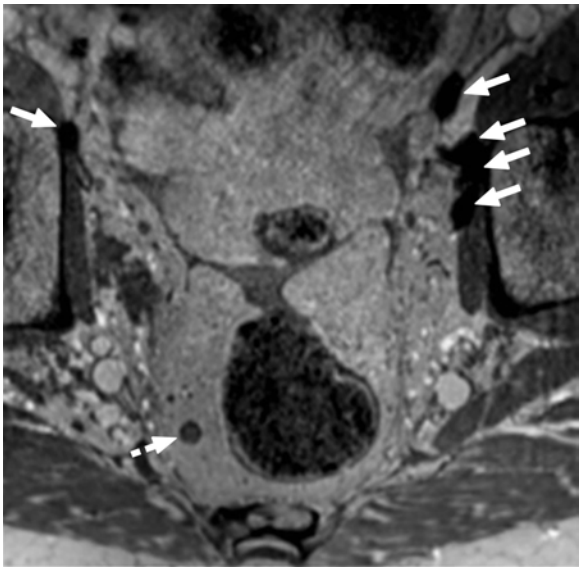

Figure 4. Functional lymph node MR imaging. USPIO-enhanced MRI in 68-year-old man with prostate cancer and pelvic lymph node metastasis. The MRI examination was performed because of rising prostate specific antigen levels after prostatectomy. Axial T1-weighted image of pelvis 24 hours after administration of USPIO particles shows that several non-metastatic lymph nodes appear "dark" (i.e. hypointense in signal intensity) (continuous arrows), whereas one metastatic lymph node appears relatively "white" (i.e. hyperintense in signal intensity) (dashed arrow). Images courtesy of Thomas Hambrock, MD, PhD, and Jelle O. Barentsz, MD, PhD, University of Nijmegen Medical Center, Nijmegen, The Netherlands.

size criteria (48-50). This can be explained by the fact that malignant tissue generally exhibits hypercellularity, increased nucleus-to-cytoplasm ratios, and an increased amount of macromolecular proteins, resulting in decreased diffusivity in the extra- and intracellular compartments. Nevertheless, ADCs of metastatic and non-metastatic lymph nodes overlap (48-50). Furthermore, other studies even reported that there was no significant difference between ADCs of metastatic and those of non-metastatic lymph nodes (51, 52). Another issue is that ADC measurements of smaller lymph nodes may be less reliable due to the image distortion, insufficient spatial resolution, and partial volume effects. Therefore, the value of ADC measurements in the assessment of lymph nodes is still questionable.

4. FUNCTIONAL IMAGING OF TUMOR MOLECULAR PROCESSES

4.1 Metabolic imaging

4.1.1. Glucose metabolism

FDG is by far the most commonly used PET tracer in the world. PET/CT is often regarded as the ''one-stop shop'' for many malignancies due to the versatility of this radiotracer which allows for accurate localization of sites of disease with unprecedented sensitivity. It is a glucose analogue first tested in humans in 1976 at the Hospital of the University of Pennsylvania (53). The mechanism of localization of FDG is well established: FDG is transported into cells via glucose transporters such as GLUT-1 and subsequently phosphorylated by hexokinase, both of which are overexpressed in the malignant cells. These two factors together with reduced or absent glucose-6-phosphatase levels in the cancer cells lead to the accumulation of the metabolic product 2-^{18}F-fluoro-2-deoxy-D-glucose-6-phosphate intracellularly, as it cannot undergo further metabolism through the glycolytic pathway. Persistent glucose uptake in many cancer cells in a low serum insulin state makes FDG an ideal tracer for cancer imaging. In addition to providing certain unique functional information, FDG-P*Et al*so provides complementary information to structural imaging techniques for the management of a wide variety of malignancies. Improved disease staging, treatment planning, and response monitoring are some of the most useful aspects of this powerful imaging technique (Figure 5).

4.1.2. Amino acid metabolism

Amino acid analogues, such as those of methionine, tyrosine, and L-dihydroxyphenylalanine (L-DOPA) have been found to be clinically useful radiotracers. Tumor imaging with amino acid analogue radiotracers allows assessment of more specific uptake in tumors, since FDG-PET is known to show nonspecific uptake in inflammatory cells and granulation tissue. Rau *et al* compared the tyrosine analogue O- (2-^{18}F-fluoroethyl)-L-tyrosine (FET) with ^{11}C-methionine (MET) and FDG in animal models and demonstrated no uptake of FET in sites of acute or chronic inflammation (54).

Advantages of imaging brain tumors with MET are due to the low background uptake of MET in the brain. However, the major shortcoming of MET is the 20-minute half-life of the ^{11}C isotope, which requires an on-site cyclotron for imaging. Jacobs *et al* showed a sensitivity of 91% for detecting gliomas, as well as larger detected tumor volumes compared with those detected with Gd-enhanced MRI, which may have an impact on radiation treatment planning (55). In one of the earliest comparative study between FET-PET and FDG-PET in peripheral tumors, it was observed that FET-PET accumulated in squamous head and neck tumors while adenocarcinomas and lymphomas exhibited no significant FET uptake (56). ^{18}F-6-fluorodihydroxyphenylalanine (FDOPA), an analogue of L-DOPA, accumulates in dopaminergic neurons in the basal ganglia and can be used to study patients with melanoma, carcinoid tumor, medullary thyroid cancer, and brain tumors (Figure 6) (57). This radiotracer has also been shown to be an important tracer for evaluation of low-grade and recurrent brain tumors and for differentiation of low-grade tumors from necrosis (58).

4.2 Cell proliferation imaging

3'-deoxy-3'-^{18}F-fluorothymidine (FLT) is a thymidine analogue that has been developed as a PET tracer to assess cell proliferation *in vivo*. The cellular mechanism of FLT uptake is that it reflects thymidine kinase-1 (TK1) activity, an enzyme expressed during the DNA synthesis phase of the cell cycle (59). The activity of

Figure 5. Glucose metabolism imaging. Whole-body ^{18}F-FDG-PET/CT in 62-year-old woman with recurrent lung cancer for restaging purposes. Coronal maximal intensity projection image reveals multiple "dark" FDG avid metastases involving thoracic lymph nodes and bone marrow. Image courtesy of Thomas C. Kwee, MD, University Medical Center Utrecht, Utrecht, The Netherlands.

the enzyme is enhanced in proliferating cells. FLT is phosphorylated by TK1, forming negatively charged FLT monophosphate, resulting in intracellular trapping. FLT uptake correlated significantly with the Ki-67 cell proliferation index in brain gliomas. Significant correlations of quantitative FLT uptake with Ki-67 have also been demonstrated in lung cancer, colorectal cancer, and lymphoma (60). FLT as a PET radiotracer has been investigated in several extracranial tumors, such as human lung cancer, colorectal cancer, melanoma, lymphoma, breast cancer, laryngeal cancer, and soft-tissue sarcomas. The studies have showed the role of FLT-PET in early monitoring of therapy response (both in chemotherapy and radiation treatment) (61, 62). Hence, there is potential for FLT-PET to shorten the time frame of detecting response to therapy, which might be an effective tool for monitoring treatment.

4.3. Oxygenation imaging

Tumor hypoxia is recognized as an important prognostic index in clinical oncology, and there has been great interest for non-invasive imaging of the oxygenation status and presence of hypoxia in malignant tissues. Hypoxic tumor cells are generally more radioresistant and chemoresistant than normoxic tumor cells (63, 64). Hence, detection and quantification of hypoxia could be used to select and plan these treatments, especially radiotherapy. ^{18}F-fluoromisonidazole (FMISO) was the first labeled nitroimidazole compound detected by PET (65). Nitroimidazole compounds undergo intracellular chemical reduction, and under chronic hypoxia their reduced moieties covalently bind to macromolecules, mainly thiol-containing proteins. FMISO has been relatively widely evaluated in non-small cell lung cancers, gliomas, and head and neck tumors, and can also be used to evaluate the penumbra following acute ischemic stroke (Figure 7). ^{64}Cu (II)-diacetyl-bis (N4-methylthiosemicarbazone) (^{64}Cu-ATSM) and ^{18}F-EF5, a 2-nitroimidazole analogue, are other newer PET radiotracers used to image hypoxia. Hypoxic regions delineated by ^{18}F-EF5-PET have been shown to predict patient survival and lack of response to radiation treatment, and preliminary tests of ^{18}F-EF5 in patients with head and neck and brain tumors show promising results (66, 67).

Various functional MRI (fMRI) techniques have been used non-invasively to study oxygenation in human tumors and to monitor changes in tumors related to therapy. These include blood oxygen level-dependent (BOLD) fMRI, Overhauser-enhanced MRI, and electron paramagnetic resonance imaging (EPRI). Advantages include potentially reducing the time of surgery and minimizing intraoperative cortical stimulation methods, which are sometimes used during the surgical resection of brain tumors (68, 69).

4.4. Molecular imaging with targeted imaging agents

4.4.1. Somatostatin receptor imaging

Receptor targeting is an attractive approach for non-invasive imaging including that of cancer. Somatostatin receptors (SSTRs) are overexpressed in many tumors (e.g., in neuroendocrine, lung, and breast tumors and in lymphomas), with subtype specificity for each histology. Five receptor subtypes (SSTR1–5), acting through transmembrane domain G proteins, have been identified. The most commonly used agent in earlier times has been ^{111}In-pentetreotide for SPECT imaging, although SSTR-targeted radiotracers have also been developed for PET, including ^{68}Ga-DOTA-Phe^{1}-Tyr^{3}-octreotide (^{68}Ga-DOTATOC) and Gluc-Lys (^{18}F-fluoropropionyl-TOCA). The PET radiotracers are of substantial value for the evaluation of patients with SSTR-positive lesions such as neuroendocrine tumors, especially carcinoid. ^{68}Ga-DOTATOC seems to be a very promising new PET radiotracer for imaging SSTRs even in small meningiomas, offering excellent imaging properties and a very high

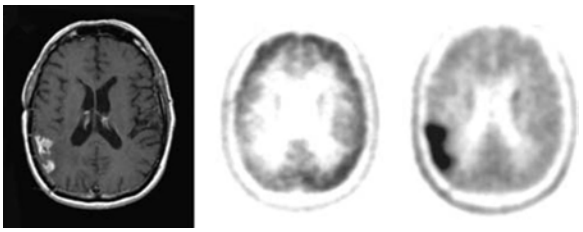

Figure 6. Amino acid uptake imaging.Gadolinium-enhanced T1-weighted MRI (left), ^{18}F-FDG-PET (middle), and ^{18}F-DOPA-PET (right) in recurrent glioblastoma multiforme. Reproduced with permission from (58).

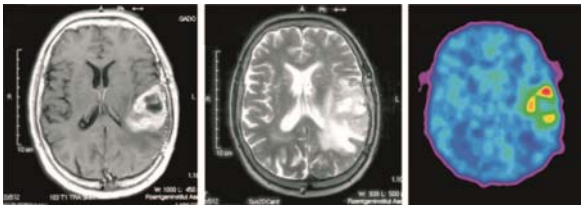

Figure 7. Hypoxia imaging.Gadolinium contrast-enhanced T1-weighted MRI (left) and T2-weighted MRI (middle) in patient with residual/recurrent glioblastoma multiforme. PET image (right) shows ^{18}F-FMISO tumor uptake 150-170 minutes after injection, indicating presence of hypoxia. Reproduced with permission from (112).

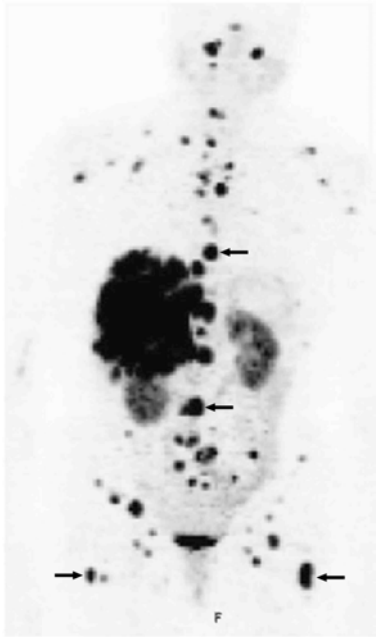

Figure 8. SSTR imaging. ^{68}Ga-DOTA-TOC in 56-year-old woman with multiple liver and lymph node metastases was referred for restaging after surgery and chemotherapy. CT (not shown) presented these tumor lesions; however, it was negative for bone lesions. Besides the visceral metastases, several additional osteoblastic and osteolytic bone marrow metastases are clearly depicted with ^{68}Ga-DOTA-TOC (arrows point to several representative osseous metastases within spine and proximal femora). Reproduced and modified with permission from (113).

tumor-to-background ratio (Figure 8). Compared with ^{111}In-pentetreotide SPECT, Gluc-Lys (^{18}F-fluoropropionyl-TOCA)-PET revealed more than twice the number of lesions and resulted in near-perfect interobserver agreement (70). ^{68}Ga-DOTA-Tyr^3-Thr^8-octreotide (^{68}Ga-DOTATATE) (an SSTR2-selective ligand) and ^{68}Ga-DOTA-1-NaI$_3$-octreotide (^{68}Ga-DOTANOC) (with SSTR2, 3, and 5 affinity) are newer somatostatin receptor imaging agents, which are currently under clinical evaluation.

4.4.2. Estrogen receptor imaging

Estrogen receptor (ER) expression in breast carcinoma is an indicator of prognosis and likelihood of response to anti-estrogen therapy. Currently, treatment with anti-estrogen therapy depends on the results of *in vitro* immunohistochemistry assays of biopsy material for ER expression in breast cancer. However, the *in vitro* assay cannot discriminate between functional and non-functional receptors. ER targeting radiotracers, therefore, may be used to non-invasively assess the functional ER status of tumors *in vivo* through use of ^{18}F fluorinated estrogen analogues, and6α-^{18}F-fluoroestradiol-17β (FES) is commonly used for this purpose due to its favorable biodistribution. FES has shown the most promise in quantifying the functional ER status of breast cancer, both in the primary tumor and in metastatic sites. Studies have shown that the quantitative level of FES uptake in primary tumors correlates with the level of ER expression measured by *in vitro* assay by radioligand binding and in preliminary data by immunohistochemistry. This PET radiotracer also provides sufficient image quality to image metastatic lesions with high sensitivity in patients with ER positive tumors (71). In addition to aiding in selection of patients for anti-estrogen therapy, FES-PET may show a faster treatment response to tamoxifen than FDG-PET at 7 to 10 days after treatment initiation (72, 73).

4.5. Angiogenesis imaging

Detection of $\alpha_V\beta_3$ integrins that are present on activated endothelial cells involved in angiogenesis can be performed by using peptides containing the amino acid sequence arginine-glycine-aspartate (RGD) that have a general affinity toward integrins. ^{18}F-galacto-RGD uptake has been found to correlate with $\alpha_V\beta_3$ expression, as well as microvessel density as observed at histology (74). This radiotracer has been postulated to have applications for individualized treatment planning and anti-angiogenic therapy monitoring, since activated endothelium is susceptible to anti-angiogenic therapy whereas quiescent endothelium is resistant to anti-angiogenic therapy (Figure 9). A drawback is that it binds to $\alpha_V\beta_3$ integrins present on the membranes of tumor cells, as well as membranes of tumor-associated endothelial cells. To circumvent this problem and to more specifically target the vascular endothelial cells, imaging agents based on targeting of cell receptors, such as vascular endothelial cell growth factor receptor, which are over-expressed on endothelial cells during angiogenesis are currently under development.

4.6. Apoptosis imaging

Annexin V is a 36-kDa protein that binds with high affinity to phosphatidylserine found on the exterior of the

Figure 9. Angiogenesis imaging. ^{18}F-galacto-RGD-PET in 70-year-old woman with invasive ductal breast cancer of left breast (arrow, open tip, solid line), axillary lymph-node metastases on left side (arrows, open tips, dotted lines), and osseous metastasis to sternum (arrow, closed tip, solid line). Reproduced with permission from (114).

cell membrane in the early stages of apoptosis. Apoptosis plays an important role in defining the biology of cancer cells. Cells deficient in apoptotic response can potentially become tumorigenic (75) . The majority of therapeutic approaches against cancer kill tumor cells by inducing programmed cell death causing DNA damage beyond the repair capability of the cell. The high-affinity binding of Annexin V to externalized phosphatidylserine makes it a sensitive probe of the early phase of apoptosis. Annexin V can be labeled with either ^{99m}Tc, ^{124}I, or ^{18}F to image apoptosis *in vivo* using SPECT or PET, respectively. These radiotracers have been studied in animal models, and such studies have shown that they can accurately measure internal levels of apoptosis non-invasively.

Superparamagnetic iron-based contrast agents and other paramagnetic contrast agents in conjunction with carrier nanoparticles that specifically target particular molecules or biologic processes of interest have been studied using MRI (76, 77). For example, Schellenberger *et al* have used nanoparticles conjugated to Annexin V to target apoptosis for non-invasive tumor monitoring using MRI (78). However, limitations of such approaches using MRI are apparent and include low signal-to-noise ratios (SNR) with low sensitivity, lack of standardization of utilized imaging sequences and parameters, lack of standardization of analysis methodologies for quantification, as well as potential toxicity of the contrast agents.

4.7 .Magnetic resonance spectroscopy

Magnetic resonance spectroscopy (MRS) is a molecular imaging method that allows for separation of the MRI signal from a given tissue into its different chemical components. This is possible because the magnetic field experienced by an atomic nucleus is minutely "shielded" or modified by the fields produced by neighboring atoms on the same molecule. This produces a "chemical shift" or small variation in the nuclear resonant frequency. As such, a display of MRI signal amplitude as a function of nuclear resonance frequency forms a spectrum, with different chemical environments of a particular type of atomic nucleus within and between molecules forming peaks at characteristic chemical shift positions. As such, it is possible to quantitatively assess the amount, type, and location of small molecular compounds within a tissue or organ of interest at the same time conventional MRI is performed (79). The data are typically displayed as a grid of spectra of chemical compound abundances obtained at either single or multiple locations in a tissue or organ of interest. These spectra are collected from spinning nuclei (spins), most often ^{1}H given the abundance of water in tissue.

^{1}H MRS enables accurate quantitative assessment of the spatial distribution of tissue metabolites such as creatinine, choline, amino acids, nucleotides, lactate, and lipids (80). Although nonspecific for cancer, there are several MRS findings that are more frequently seen in cancer. For example, increased concentrations of cell membrane metabolites like phosphocholine may be seen due to increased membrane synthesis, a higher concentration of lactate may be seen due to increased metabolism through the glycolytic pathway, and lower concentrations of normal tissue metabolites (such as N-acetyl aspartate in cerebral tissue or citrate in prostatic tissue) may be encountered (81, 82). In both research and clinical practice, ^{1}H MRS is most frequently applied in the brain, given the relative lack of motion in this location compared to other body regions. ^{1}H MRS has been reported to be useful for the characterization of brain tumors (including the differentiation between pyogenic brain abscesses from cystic or necrotic brain tumors, and the discrimination between gliomas and solitary brain metastases) (83, 84) and grading of gliomas (85). Furthermore, ^{1}H MRS may provide a more accurate assessment of tumor cell infiltration than structural imaging alone (86, 87). This, in turn, has significant implications for surgery and/or radiotherapy planning. In addition, ^{1}H MRS may be useful to predict patient prognosis; it has been reported that patients with glioblastoma multiforme had significantly shorter median survival when a large volume

of metabolic abnormality was seen at ^{1}H MRS (88). Finally, studies have shown that ^{1}H MRS can be used to discriminate residual or recurrent brain tumor from post-radiation changes (89, 90). Several studies also investigated the utility of ^{1}H MRS for the evaluation of extracranial tumors, including tumors of the breast, pancreas, adrenals, cervix, prostate, bone, and soft-tissue (91-96). However, it is beyond the scope of this scientific communication to provide an in-depth overview of the literature on the use of ^{1}H MRS in oncology, and the reader is referred to a previous review article on this topic (80).

It is of interest to note that there is an increasing trend towards performing MRI at higher field strengths (>1.5 T), because signal-to-noise ratio (SNR) increases linearly with field strength (97). Increasing the field strength may also be of advantage for MRS. First, more signal intensity can be detected from a given volume per unit of scan time, and, second, the frequency dispersion (chemical shift) allowing one to distinguish several lines in the spectra is also increased (97). The increased chemical shift may not only improve the accuracy of the determination of compounds that are also seen at lower field strengths, but it may also allow detection of other compounds which may be used as biomarkers for the evaluation of tumors. Recently, whole-body MRI scanners operating at 7.0 T have become available (98), and research in this field is very active. Although several technical challenges still have to be overcome, the first MRS studies at 7.0 T are promising and confirm the theoretical advantages of performing MRS at higher field strengths (99, 100). For example, a recent volunteer study (99) that compared ^{1}H MRS of the brain at 4.0 T to that at 7.0 T, reported that the spectral line width was increased by 50% at 7.0 T, which resulted in a 14% increase in spectral resolution at 7.0 T relative to 4.0 T. In addition, metabolite quantification at 7.0 T was less sensitive to reduced SNR than at 4.0 T, and the precision of metabolite quantification and detectability of weakly represented metabolites were substantially increased at 7.0 T relative to 4.0 T. Because of the increased spectral resolution at 7.0 T, only one-half of the SNR of a 4.0 T spectrum was required to obtain the same quantification precision (99). Another recent study (100) has shown that ^{1}H MRS of the prostate is feasible at 7.0T, and allowed the detection of polyamines next to citrate, creatine, and choline; these potential tumor markers may improve the *in vivo* detection, localization, and assessment of prostate cancer. Attempts are ongoing to apply 7.0 T ^{1}H MRS for the evaluation of tumors in other body regions as well.

Other nuclear candidates for MRS include ^{13}C, ^{19}F, ^{23}Na, and ^{31}P (79). Phosphorus is fundamental to a number of cellular processes, including energy metabolism and membrane construction, and has attracted a lot of attention for MRS. ^{31}P MRS offers insight into processes such as cell energy metabolism, tissue oxygenation state, pH, and membrane turnover (79). It has shown some promise to differentiate prostate carcinoma from benign prostatic hypertrophy (101). Others have shown that it can differentiate benign from malignant head and neck neoplasms, can predict treatment response, and demonstrate therapeutic effects in head and neck cancer (102). It has also been reported that ^{31}P MRS pre-treatment measurement of phosphoethanolamine and phosphocholine content within non-Hodgkin's lymphoma predicts long-term response to treatment and time-to-treatment failure, particularly when combined with the international prognostic index (103).

Another exciting development is the use of hyperpolarized contrast agents for molecular and metabolic imaging (104, 105). Hyperpolarization is the general term for a method of enhancing the spin-polarization difference of populations of nuclei in a magnetic field. Since signal intensity and SNR depend linearly upon polarization level, this method makes it possible to visualize heteronuclei (i.e. atomic nuclei other than ^{1}H) that are normally not abundant and/or have a low concentration in the human body. Although all heteronuclei can be hyperpolarized, at the moment only ^{13}C has been used for *in vivo* MRI experiments. This is due to the relatively high gyromagnetic ratio (a constant for a specific nucleus that relates the nuclear magnetic resonance frequency and the strength of the external magnetic field) of ^{13}C, which increases its sensitivity, and to availability of dedicated coils tuned to the ^{13}C frequency. The highly increased signal intensity that can be achieved through hyperpolarization makes it possible to detect newly formed ^{13}C compounds in very short times after injection of a hyperpolarized ^{13}C contrast agent without background signal. This makes the visualization of molecules that represent key steps of the cellular metabolism possible, therefore providing a direct access to physiological/pathological changes at the cellular level. Using chemical shift imaging sequences, more than one molecule can be visualized in the same anatomical region (104, 105). For example, animal studies have shown that it is possible to obtain maps of pyruvate, lactate, and alanine within a time frame of <1 minute after the intravenous administration of ^{13}C-hyperpolarized pyruvate, and reported that tumors have a higher lactate concentration than normal tissue and that lactate SNR levels may be correlated to histological grade (106-108). The hyperpolarized ^{13}C-pyruvate technique may also be used for detecting tumor response to treatment, as was shown in *in vitro* and animal studies in lymphoma which reported that the conversion of pyruvate to lactate in the tumor is reduced following treatment (109), and may be an alternative to FDG-PET for imaging tumor treatment response (110). Besides hyperpolarized ^{13}C-pyruvate, several other ^{13}C-hyperpolarized molecules that may enhance our understanding of tumor biology at the molecular/metabolic level and that may improve the evaluation of cancerous lesions are currently being investigated (104, 105). An important prerequisite for MRS-based molecular/metabolic imaging methods to be widely accepted in routine clinical practice is standardization of acquisition and analysis protocols.

5. CONCLUSION

A wide variety of functional imaging techniques is available for visualizing and quantifying tumor

physiology and tumor molecular processes *in vivo*. Combined with structural imaging techniques, functional imaging may improve the efficiency and effectiveness of research in oncology, will help to characterize biomarkers of disease and new endpoints for assessment of tumor response, and, eventually, reduce cancer-related morbidity and mortality by improving cancer screening, diagnosis and staging, prognosis assessment, image-guided treatment, assessment of treatment response, and detection of tumor recurrence. Further research is warranted to establish the clinical value and/or to optimize the clinical use of the functional imaging techniques that have been described in this review.

6. ACKNOWLEDGEMENT

Thomas C. Kwee, Sandip Basu have contributed equally to this manuscript.

7. REFERENCES

1. A. Jemal, R. Siegel, J. Xu and E. Ward: Cancer statistics, 2010. *CA Cancer J Clin*, 60(5), 277-300 (2010)

2. D. A. Torigian, S. S. Huang, M. Houseni and A. Alavi: Functional imaging of cancer with emphasis on molecular techniques. *CA Cancer J Clin*, 57(4), 206-24 (2007)

3. J. Barentsz, S. Takahashi, W. Oyen, R. Mus, P. De Mulder, R. Reznek, M. Oudkerk and W. Mali: Commonly used imaging techniques for diagnosis and staging. *J Clin Oncol*, 24(20), 3234-44 (2006)

4. M. Schnall and M. Rosen: Primer on imaging technologies for cancer. *J Clin Oncol*, 24(20), 3225-33 (2006)

5. M. Atri: New technologies and directed agents for applications of cancer imaging. *J Clin Oncol*, 24(20), 3299-308 (2006)

6. D. W. Townsend: Dual-modality imaging: combining anatomy and function. *J Nucl Med*, 49(6), 938-55 (2008)

7. J. Folkman: Tumor angiogenesis: therapeutic implications. *N Engl J Med*, 285(21), 1182-6 (1971)

8. V. Goh and A. R. Padhani: Imaging tumor angiogenesis: functional assessment using MDCT or MRI? *Abdom Imaging*, 31(2), 194-9 (2006)

9. A. R. Padhani: Dynamic contrast-enhanced MR imaging. *Cancer Imaging*, 1, 52-63 (2000)

10. N. Hylton: Dynamic contrast-enhanced magnetic resonance imaging as an imaging biomarker. *J Clin Oncol*, 24(20), 3293-8 (2006)

11. E. Stejskal and J. Tanner: Spin diffusion measurements: spin echoes in the presence of a time-dependent field gradient. . *J Chem Phys*, 42, 288-292 (1965)

12. P. W. Schaefer, P. E. Grant and R. G. Gonzalez: Diffusion-weighted MR imaging of the brain. *Radiology*, 217(2), 331-45 (2000)

13. D. M. Koh and D. J. Collins: Diffusion-weighted MRI in the body: applications and challenges in oncology. *AJR Am J Roentgenol*, 188(6), 1622-35 (2007)

14. A. R. Padhani, G. Liu, D. M. Koh, T. L. Chenevert, H. C. Thoeny, T. Takahara, A. Dzik-Jurasz, B. D. Ross, M. Van Cauteren, D. Collins, D. A. Hammoud, G. J. Rustin, B. Taouli and P. L. Choyke: Diffusion-weighted magnetic resonance imaging as a cancer biomarker: consensus and recommendations. *Neoplasia*, 11(2), 102-25 (2009)

15. T. Takahara, Y. Imai, T. Yamashita, S. Yasuda, S. Nasu and M. Van Cauteren: Diffusion weighted whole body imaging with background body signal suppression (DWIBS): technical improvement using free breathing, STIR and high resolution 3D display. *Radiat Med*, 22(4), 275-82 (2004)

16. H. Nomori, T. Mori, K. Ikeda, K. Kawanaka, S. Shiraishi, K. Katahira and Y. Yamashita: Diffusion-weighted magnetic resonance imaging can be used in place of positron emission tomography for N staging of non-small cell lung cancer with fewer false-positive results. *J Thorac Cardiovasc Surg*, 135(4), 816-22 (2008)

17. Y. Ohno, H. Koyama, Y. Onishi, D. Takenaka, M. Nogami, T. Yoshikawa, S. Matsumoto, Y. Kotani and K. Sugimura: Non-small cell lung cancer: whole-body MR examination for M-stage assessment--utility for whole-body diffusion-weighted imaging compared with integrated FDG PET/CT. *Radiology*, 248(2), 643-54 (2008)

18. D. Takenaka, Y. Ohno, K. Matsumoto, N. Aoyama, Y. Onishi, H. Koyama, M. Nogami, T. Yoshikawa, S. Matsumoto and K. Sugimura: Detection of bone metastases in non-small cell lung cancer patients: comparison of whole-body diffusion-weighted imaging (DWI), whole-body MR imaging without and with DWI, whole-body FDG-PET/CT, and bone scintigraphy. *J Magn Reson Imaging*, 30(2), 298-308 (2009)

19. R. Murakami, T. Hirai, T. Sugahara, H. Fukuoka, R. Toya, S. Nishimura, M. Kitajima, T. Okuda, H. Nakamura, N. Oya, J. Kuratsu and Y. Yamashita: Grading astrocytic tumors by using apparent diffusion coefficient parameters: superiority of a one- versus two-parameter pilot method. *Radiology*, 251(3), 838-45 (2009)

20. T. Mori, H. Nomori, K. Ikeda, K. Kawanaka, S. Shiraishi, K. Katahira and Y. Yamashita: Diffusion-weighted magnetic resonance imaging for diagnosing malignant pulmonary nodules/masses: comparison with positron emission tomography. *J Thorac Oncol*, 3(4), 358-64 (2008)

21. Y. Ohba, H. Nomori, T. Mori, K. Ikeda, H. Shibata, H. Kobayashi, S. Shiraishi and K. Katahira: Is diffusion-weighted magnetic resonance imaging superior to positron emission tomography with fludeoxyglucose F 18 in imaging non-small cell lung cancer? *J Thorac Cardiovasc Surg*, 138(2), 439-45 (2009)

22. M. Nakajo, Y. Kajiya, T. Kaneko, Y. Kaneko, T. Takasaki, A. Tani, M. Ueno and C. Koriyama: FDG PET/CT and diffusion-weighted imaging for breast cancer: prognostic value of maximum standardized uptake values and apparent diffusion coefficient values of the primary lesion. *Eur J Nucl Med Mol Imaging*, 37(11), 2011-20 (2010)

23. D. A. Hamstra, A. Rehemtulla and B. D. Ross: Diffusion magnetic resonance imaging: a biomarker for treatment response in oncology. *J Clin Oncol*, 25(26), 4104-9 (2007)

24. D. A. Hamstra, C. J. Galban, C. R. Meyer, T. D. Johnson, P. C. Sundgren, C. Tsien, T. S. Lawrence, L. Junck, D. J. Ross, A. Rehemtulla, B. D. Ross and T. L. Chenevert: Functional diffusion map as an early imaging biomarker for high-grade glioma: correlation with conventional radiologic response and overall survival. *J Clin Oncol*, 26(20), 3387-94 (2008)

25. C. J. Galban, S. K. Mukherji, T. L. Chenevert, C. R. Meyer, D. A. Hamstra, P. H. Bland, T. D. Johnson, B. A. Moffat, A. Rehemtulla, A. Eisbruch and B. D. Ross: A feasibility study of parametric response map analysis of diffusion-weighted magnetic resonance imaging scans of head and neck cancer patients for providing early detection of therapeutic efficacy. *Transl Oncol*, 2(3), 184-90 (2009)

26. B. Ma, C. R. Meyer, M. D. Pickles, T. L. Chenevert, P. H. Bland, C. J. Galban, A. Rehemtulla, L. W. Turnbull and B. D. Ross: Voxel-by-voxel functional diffusion mapping for early evaluation of breast cancer treatment. *Inf Process Med Imaging*, 21, 276-87 (2009)

27. K. C. Lee, D. A. Bradley, M. Hussain, C. R. Meyer, T. L. Chenevert, J. A. Jacobson, T. D. Johnson, C. J. Galban, A. Rehemtulla, K. J. Pienta and B. D. Ross: A feasibility study evaluating the functional diffusion map as a predictive imaging biomarker for detection of treatment response in a patient with metastatic prostate cancer to the bone. *Neoplasia*, 9(12), 1003-11 (2007)

28. C. Beaulieu: The basis of anisotropic water diffusion in the nervous system - a technical review. *NMR Biomed*, 15(7-8), 435-55 (2002) doi:10.1002/nbm.782

29. P. Hagmann, L. Jonasson, P. Maeder, J. P. Thiran, V. J. Wedeen and R. Meuli: Understanding diffusion MR imaging techniques: from scalar diffusion-weighted imaging to diffusion tensor imaging and beyond. *Radiographics*, 26 Suppl 1, S205-23 (2006)

30. C. Nimsky, O. Ganslandt, P. Hastreiter, R. Wang, T. Benner, A. G. Sorensen and R. Fahlbusch: Preoperative and intraoperative diffusion tensor imaging-based fiber tracking in glioma surgery. *Neurosurgery*, 56(1), 130-7; discussion 138 (2005)

31. C. Nimsky, O. Ganslandt, P. Hastreiter, R. Wang, T. Benner, A. G. Sorensen and R. Fahlbusch: Intraoperative diffusion-tensor MR imaging: shifting of white matter tracts during neurosurgical procedures--initial experience. *Radiology*, 234(1), 218-25 (2005)

32. C. Nimsky, O. Ganslandt, P. Hastreiter, R. Wang, T. Benner, A. G. Sorensen and R. Fahlbusch: Preoperative and intraoperative diffusion tensor imaging-based fiber tracking in glioma surgery. *Neurosurgery*, 61(1 Suppl), 178-85; discussion 186 (2007)

33. Y. K. Mariappan, K. J. Glaser and R. L. Ehman: Magnetic resonance elastography: a review. *Clin Anat*, 23(5), 497-511 (2010)

34. R. Muthupillai, D. J. Lomas, P. J. Rossman, J. F. Greenleaf, A. Manduca and R. L. Ehman: Magnetic resonance elastography by direct visualization of propagating acoustic strain waves. *Science*, 269(5232), 1854-7 (1995)

35. L. Huwart, C. Sempoux, E. Vicaut, N. Salameh, L. Annet, E. Danse, F. Peeters, L. C. ter Beek, J. Rahier, R. Sinkus, Y. Horsmans and B. E. Van Beers: Magnetic resonance elastography for the noninvasive staging of liver fibrosis. *Gastroenterology*, 135(1), 32-40 (2008)

36. T. A. Krouskop, P. S. Younes, S. Srinivasan, T. Wheeler and J. Ophir: Differences in the compressive stress-strain response of infiltrating ductal carcinomas with and without lobular features--implications for mammography and elastography. *Ultrason Imaging*, 25(3), 162-70 (2003)

37. R. Sinkus, K. Siegmann, T. Xydeas, M. Tanter, C. Claussen and M. Fink: MR elastography of breast lesions: understanding the solid/liquid duality can improve the specificity of contrast-enhanced MR mammography. *Magn Reson Med*, 58(6), 1135-44 (2007)

38. M. Torabi, S. L. Aquino and M. G. Harisinghani: Current concepts in lymph node imaging. *J Nucl Med*, 45(9), 1509-18 (2004)

39. J. F. Thompson and R. F. Uren: Lymphatic mapping in management of patients with primary cutaneous melanoma. *Lancet Oncol*, 6(11), 877-85 (2005)

40. J. R. Benson, I. Jatoi, M. Keisch, F. J. Esteva, A. Makris and V. C. Jordan: Early breast cancer. *Lancet*, 373(9673), 1463-79 (2009)

41. V. Ficarra and A. Galfano: Should the dynamic sentinel node biopsy (DSNB) be considered the gold standard in the evaluation of lymph node status in patients with penile carcinoma? *Eur Urol*, 52(1), 17-9; discussion 20-1 (2007)

42. B. J. Czerniecki, I. Bedrosian, M. Faries and A. Alavi: Revolutionary impact of lymphoscintigraphy and

intraoperative sentinel node mapping in the clinical practice of oncology. *Semin Nucl Med*, 31(2), 158-64 (2001)

43. T. K. Lam, R. F. Uren, R. A. Scolyer, M. J. Quinn, K. F. Shannon and J. F. Thompson: False-negative sentinel node biopsy because of obstruction of lymphatics by metastatic melanoma: the value of ultrasound in conjunction with preoperative lymphoscintigraphy. *Melanoma Res*, 19(2), 94-9 (2009)

44. A. Goyal, A. G. Douglas-Jones, R. G. Newcombe and R. E. Mansel: Effect of lymphatic tumor burden on sentinel lymph node biopsy in breast cancer. *Breast J*, 11(3), 188-94 (2005)

45. J. A. Leijte, I. M. van der Ploeg, R. A. Valdes Olmos, O. E. Nieweg and S. Horenblas: Visualization of tumor blockage and rerouting of lymphatic drainage in penile cancer patients by use of SPECT/CT. *J Nucl Med*, 50(3), 364-7 (2009)

46. R. Weissleder, G. Elizondo, J. Wittenberg, A. S. Lee, L. Josephson and T. J. Brady: Ultrasmall superparamagnetic iron oxide: an intravenous contrast agent for assessing lymph nodes with MR imaging. *Radiology*, 175(2), 494-8 (1990)

47. O. Will, S. Purkayastha, C. Chan, T. Athanasiou, A. W. Darzi, W. Gedroyc and P. P. Tekkis: Diagnostic precision of nanoparticle-enhanced MRI for lymph-node metastases: a meta-analysis. *Lancet Oncol*, 7(1), 52-60 (2006)

48. V. Vandecaveye, F. De Keyzer, V. Vander Poorten, P. Dirix, E. Verbeken, S. Nuyts and R. Hermans: Head and neck squamous cell carcinoma: value of diffusion-weighted MR imaging for nodal staging. *Radiology*, 251(1), 134-46 (2009)

49. J. K. Kim, K. A. Kim, B. W. Park, N. Kim and K. S. Cho: Feasibility of diffusion-weighted imaging in the differentiation of metastatic from nonmetastatic lymph nodes: early experience. *J Magn Reson Imaging*, 28(3), 714-9 (2008)

50. M. Eiber, A. J. Beer, K. Holzapfel, R. Tauber, C. Ganter, G. Weirich, B. J. Krause, E. J. Rummeny and J. Gaa: Preliminary results for characterization of pelvic lymph nodes in patients with prostate cancer by diffusion-weighted MR-imaging. *Invest Radiol*, 45(1), 15-23 (2010)

51. G. Nakai, M. Matsuki, Y. Inada, F. Tatsugami, M. Tanikake, I. Narabayashi and T. Yamada: Detection and evaluation of pelvic lymph nodes in patients with gynecologic malignancies using body diffusion-weighted magnetic resonance imaging. *J Comput Assist Tomogr*, 32(5), 764-8 (2008)

52. G. Lin, K. C. Ho, J. J. Wang, K. K. Ng, Y. Y. Wai, Y. T. Chen, C. J. Chang, S. H. Ng, C. H. Lai and T. C. Yen: Detection of lymph node metastasis in cervical and uterine cancers by diffusion-weighted magnetic resonance imaging at 3T. *J Magn Reson Imaging*, 28(1), 128-35 (2008)

53. A. Alavi, J. W. Kung and H. Zhuang: Implications of PET based molecular imaging on the current and future practice of medicine. *Semin Nucl Med*, 34(1), 56-69 (2004)

54. F. C. Rau, W. A. Weber, H. J. Wester, M. Herz, I. Becker, A. Kruger, M. Schwaiger and R. Senekowitsch-Schmidtke: O-(2-[(18)F]Fluoroethyl)- L-tyrosine (FET): a tracer for differentiation of tumour from inflammation in murine lymph nodes. *Eur J Nucl Med Mol Imaging*, 29(8), 1039-46 (2002)

55. A. H. Jacobs, A. Thomas, L. W. Kracht, H. Li, C. Dittmar, G. Garlip, N. Galldiks, J. C. Klein, J. Sobesky, R. Hilker, S. Vollmar, K. Herholz, K. Wienhard and W. D. Heiss: 18F-fluoro-L-thymidine and 11C-methylmethionine as markers of increased transport and proliferation in brain tumors. *J Nucl Med*, 46(12), 1948-58 (2005)

56. D. Pauleit, G. Stoffels, W. Schaden, K. Hamacher, D. Bauer, L. Tellmann, H. Herzog, S. Broer, H. H. Coenen and K. J. Langen: PET with O-(2-18F-Fluoroethyl)-L-Tyrosine in peripheral tumors: first clinical results. *J Nucl Med*, 46(3), 411-6 (2005)

57. S. Hoegerle, C. Altehoefer, N. Ghanem, G. Koehler, C. F. Waller, H. Scheruebl, E. Moser and E. Nitzsche: Whole-body 18F dopa PET for detection of gastrointestinal carcinoid tumors. *Radiology*, 220(2), 373-80 (2001)

58. W. Chen, D. H. Silverman, S. Delaloye, J. Czernin, N. Kamdar, W. Pope, N. Satyamurthy, C. Schiepers and T. Cloughesy: 18F-FDOPA PET imaging of brain tumors: comparison study with 18F-FDG PET and evaluation of diagnostic accuracy. *J Nucl Med*, 47(6), 904-11 (2006)

59. J. S. Rasey, J. R. Grierson, L. W. Wiens, P. D. Kolb and J. L. Schwartz: Validation of FLT uptake as a measure of thymidine kinase-1 activity in A549 carcinoma cells. *J Nucl Med*, 43(9), 1210-7 (2002)

60. A. K. Buck, G. Halter, H. Schirrmeister, J. Kotzerke, I. Wurziger, G. Glatting, T. Mattfeldt, B. Neumaier, S. N. Reske and M. Hetzel: Imaging proliferation in lung tumors with PET: 18F-FLT versus 18F-FDG. *J Nucl Med*, 44(9), 1426-31 (2003)

61. B. S. Pio, C. K. Park, R. Pietras, W. A. Hsueh, N. Satyamurthy, M. D. Pegram, J. Czernin, M. E. Phelps and D. H. Silverman: Usefulness of 3'-[F-18]fluoro-3'-deoxythymidine with positron emission tomography in predicting breast cancer response to therapy. *Mol Imaging Biol*, 8(1), 36-42 (2006)

62. D. L. Francis, D. Visvikis, D. C. Costa, T. H. Arulampalam, C. Townsend, S. K. Luthra, I. Taylor and P. J. Ell: Potential impact of [18F]3'-deoxy-3'-fluorothymidine versus [18F]fluoro-2-deoxy-D-glucose in positron emission tomography for colorectal cancer. *Eur J Nucl Med Mol Imaging*, 30(7), 988-94 (2003)

63. P. Vaupel, A. Mayer, S. Briest and M. Hockel: Hypoxia in breast cancer: role of blood flow, oxygen diffusion

distances, and anemia in the development of oxygen depletion. *Adv Exp Med Biol*, 566, 333-42 (2005)

64. J. P. Kirkpatrick, L. I. Cardenas-Navia and M. W. Dewhirst: Predicting the effect of temporal variations in PO2 on tumor radiosensitivity. *Int J Radiat Oncol Biol Phys*, 59(3), 822-33 (2004)

65. J. S. Rasey, Z. Grunbaum, S. Magee, N. J. Nelson, P. L. Olive, R. E. Durand and K. A. Krohn: Characterization of radiolabeled fluoromisonidazole as a probe for hypoxic cells. *Radiat Res*, 111(2), 292-304 (1987)

66. S. M. Evans, S. Hahn, D. R. Pook, W. T. Jenkins, A. A. Chalian, P. Zhang, C. Stevens, R. Weber, G. Weinstein, I. Benjamin, N. Mirza, M. Morgan, S. Rubin, W. G. McKenna, E. M. Lord and C. J. Koch: Detection of hypoxia in human squamous cell carcinoma by EF5 binding. *Cancer Res*, 60(7), 2018-24 (2000)

67. S. M. Evans, K. D. Judy, I. Dunphy, W. T. Jenkins, P. T. Nelson, R. Collins, E. P. Wileyto, K. Jenkins, S. M. Hahn, C. W. Stevens, A. R. Judkins, P. Phillips, B. Geoerger and C. J. Koch: Comparative measurements of hypoxia in human brain tumors using needle electrodes and EF5 binding. *Cancer Res*, 64(5), 1886-92 (2004)

68. A. R. Padhani: Where are we with imaging oxygenation in human tumours? *Cancer Imaging*, 5, 128-30 (2005)

69. M. C. Krishna, S. Subramanian, P. Kuppusamy and J. B. Mitchell: Magnetic resonance imaging for *in vivo* assessment of tissue oxygen concentration. *Semin Radiat Oncol*, 11(1), 58-69 (2001)

70. G. Meisetschlager, T. Poethko, A. Stahl, I. Wolf, K. Scheidhauer, M. Schottelius, M. Herz, H. J. Wester and M. Schwaiger: Gluc-Lys([18F]FP)-TOCA PET in patients with SSTR-positive tumors: biodistribution and diagnostic evaluation compared with [111In]DTPA-octreotide. *J Nucl Med*, 47(4), 566-73 (2006)

71. W. B. Eubank and D. A. Mankoff: Evolving role of positron emission tomography in breast cancer imaging. *Semin Nucl Med*, 35(2), 84-99 (2005)

72. F. Dehdashti, F. L. Flanagan, J. E. Mortimer, J. A. Katzenellenbogen, M. J. Welch and B. A. Siegel: Positron emission tomographic assessment of "metabolic flare" to predict response of metastatic breast cancer to antiestrogen therapy. *Eur J Nucl Med*, 26(1), 51-6 (1999)

73. H. M. Linden, S. A. Stekhova, J. M. Link, J. R. Gralow, R. B. Livingston, G. K. Ellis, P. H. Petra, L. M. Peterson, E. K. Schubert, L. K. Dunnwald, K. A. Krohn and D. A. Mankoff: Quantitative fluoroestradiol positron emission tomography imaging predicts response to endocrine treatment in breast cancer. *J Clin Oncol*, 24(18), 2793-9 (2006)

74. A. J. Beer, R. Haubner, M. Sarbia, M. Goebel, S. Luderschmidt, A. L. Grosu, O. Schnell, M. Niemeyer, H. Kessler, H. J. Wester, W. A. Weber and M. Schwaiger: Positron emission tomography using [18F]Galacto-RGD identifies the level of integrin alpha(v)beta3 expression in man. *Clin Cancer Res*, 12(13), 3942-9 (2006)

75. A. G. Knudson: Cancer genetics. *Am J Med Genet*, 111(1), 96-102 (2002)

76. I. Serganova and R. Blasberg: Reporter gene imaging: potential impact on therapy. *Nucl Med Biol*, 32(7), 763-80 (2005)

77. S. D. Caruthers, P. M. Winter, S. A. Wickline and G. M. Lanza: Targeted magnetic resonance imaging contrast agents. *Methods Mol Med*, 124, 387-400 (2006)

78. E. A. Schellenberger, D. Hogemann, L. Josephson and R. Weissleder: Annexin V-CLIO: a nanoparticle for detecting apoptosis by MRI. *Acad Radiol*, 9 Suppl 2, S310-1 (2002)

79. A. M. Aisen and T. L. Chenevert: MR spectroscopy: clinical perspective. *Radiology*, 173(3), 593-9 (1989)

80. C. Mountford, C. Lean, P. Malycha and P. Russell: Proton spectroscopy provides accurate pathology on biopsy and *in vivo*. *J Magn Reson Imaging*, 24(3), 459-77 (2006)

81. U. Sharma, A. Mehta, V. Seenu and N. R. Jagannathan: Biochemical characterization of metastatic lymph nodes of breast cancer patients by *in vitro* 1H magnetic resonance spectroscopy: a pilot study. *Magn Reson Imaging*, 22(5), 697-706 (2004)

82. J. Kurhanewicz, D. B. Vigneron and S. J. Nelson: Three-dimensional magnetic resonance spectroscopic imaging of brain and prostate cancer. *Neoplasia*, 2(1-2), 166-89 (2000)

83. W. Hollingworth, L. S. Medina, R. E. Lenkinski, D. K. Shibata, B. Bernal, D. Zurakowski, B. Comstock and J. G. Jarvik: A systematic literature review of magnetic resonance spectroscopy for the characterization of brain tumors. *AJNR Am J Neuroradiol*, 27(7), 1404-11 (2006)

84. C. Majos, C. Aguilera, J. Alonso, M. Julia-Sape, S. Castaner, J. J. Sanchez, A. Samitier, A. Leon, A. Rovira and C. Arus: Proton MR spectroscopy improves discrimination between tumor and pseudotumoral lesion in solid brain masses. *AJNR Am J Neuroradiol*, 30(3), 544-51 (2009)

85. A. Stadlbauer, S. Gruber, C. Nimsky, R. Fahlbusch, T. Hammen, R. Buslei, B. Tomandl, E. Moser and O. Ganslandt: Preoperative grading of gliomas by using metabolite quantification with high-spatial-resolution proton MR spectroscopic imaging. *Radiology*, 238(3), 958-69 (2006)

86. A. Laprie, I. Catalaa, E. Cassol, T. R. McKnight, D. Berchery, D. Marre, J. M. Bachaud, I. Berry and E. C. Moyal: Proton magnetic resonance spectroscopic imaging in newly diagnosed glioblastoma: predictive value for the

site of postradiotherapy relapse in a prospective longitudinal study. *Int J Radiat Oncol Biol Phys*, 70(3), 773-81 (2008)

87. I. Park, G. Tamai, M. C. Lee, C. F. Chuang, S. M. Chang, M. S. Berger, S. J. Nelson and A. Pirzkall: Patterns of recurrence analysis in newly diagnosed glioblastoma multiforme after three-dimensional conformal radiation therapy with respect to pre-radiation therapy magnetic resonance spectroscopic findings. *Int J Radiat Oncol Biol Phys*, 69(2), 381-9 (2007)

88. J. Oh, R. G. Henry, A. Pirzkall, Y. Lu, X. Li, I. Catalaa, S. Chang, W. P. Dillon and S. J. Nelson: Survival analysis in patients with glioblastoma multiforme: predictive value of choline-to-N-acetylaspartate index, apparent diffusion coefficient, and relative cerebral blood volume. *J Magn Reson Imaging*, 19(5), 546-54 (2004)

89. P. Weybright, P. C. Sundgren, P. Maly, D. G. Hassan, B. Nan, S. Rohrer and L. Junck: Differentiation between brain tumor recurrence and radiation injury using MR spectroscopy. *AJR Am J Roentgenol*, 185(6), 1471-6 (2005)

90. E. A. Smith, R. C. Carlos, L. R. Junck, C. I. Tsien, A. Elias and P. C. Sundgren: Developing a clinical decision model: MR spectroscopy to differentiate between recurrent tumor and radiation change in patients with new contrast-enhancing lesions. *AJR Am J Roentgenol*, 192(2), W45-52 (2009)

91. L. Bartella, E. A. Morris, D. D. Dershaw, L. Liberman, S. B. Thakur, C. Moskowitz, J. Guido and W. Huang: Proton MR spectroscopy with choline peak as malignancy marker improves positive predictive value for breast cancer diagnosis: preliminary study. *Radiology*, 239(3), 686-92 (2006)

92. S. G. Cho, D. H. Lee, K. Y. Lee, H. Ji, K. H. Lee, P. R. Ros and C. H. Suh: Differentiation of chronic focal pancreatitis from pancreatic carcinoma by *in vivo* proton magnetic resonance spectroscopy. *J Comput Assist Tomogr*, 29(2), 163-9 (2005)

93. J. F. Faria, S. M. Goldman, J. Szejnfeld, H. Melo, C. Kater, P. Kenney, M. P. Huayllas, G. Demarchi, V. V. Francisco, C. Andreoni, M. Srougi, V. Ortiz and N. Abdalla: Adrenal masses: characterization with *in vivo* proton MR spectroscopy--initial experience. *Radiology*, 245(3), 788-97 (2007)

94. M. M. Mahon, A. D. Williams, W. P. Soutter, I. J. Cox, G. A. McIndoe, G. A. Coutts, R. Dina and N. M. deSouza: 1H magnetic resonance spectroscopy of invasive cervical cancer: an *in vivo* study with *ex vivo* corroboration. *NMR Biomed*, 17(1), 1-9 (2004)

95. P. Swindle, S. McCredie, P. Russell, U. Himmelreich, M. Khadra, C. Lean and C. Mountford: Pathologic characterization of human prostate tissue with proton MR spectroscopy. *Radiology*, 228(1), 144-51 (2003)

96. C. K. Wang, C. W. Li, T. J. Hsieh, S. H. Chien, G. C. Liu and K. B. Tsai: Characterization of bone and soft-tissue tumors with *in vivo* 1H MR spectroscopy: initial results. *Radiology*, 232(2), 599-605 (2004)

97. F. Schick: Whole-body MRI at high field: technical limits and clinical potential. *Eur Radiol*, 15(5), 946-59 (2005)

98. J. T. Vaughan, C. J. Snyder, L. J. DelaBarre, P. J. Bolan, J. Tian, L. Bolinger, G. Adriany, P. Andersen, J. Strupp and K. Ugurbil: Whole-body imaging at 7T: preliminary results. *Magn Reson Med*, 61(1), 244-8 (2009)

99. I. Tkac, G. Oz, G. Adriany, K. Ugurbil and R. Gruetter: *In vivo* 1H NMR spectroscopy of the human brain at high magnetic fields: metabolite quantification at 4T vs. 7T. *Magn Reson Med*, 62(4), 868-79 (2009)

100. D. W. Klomp, A. K. Bitz, A. Heerschap and T. W. Scheenen: Proton spectroscopic imaging of the human prostate at 7 T. *NMR Biomed*, 22(5), 495-501 (2009)

101. P. Narayan, P. Jajodia, J. Kurhanewicz, A. Thomas, J. MacDonald, B. Hubesch, M. Hedgcock, C. M. Anderson, T. L. James, E. A. Tanagho and *et al.*: Characterization of prostate cancer, benign prostatic hyperplasia and normal prostates using transrectal 31phosphorus magnetic resonance spectroscopy: a preliminary report. *J Urol*, 146(1), 66-74 (1991)

102. A. Shukla-Dave, H. Poptani, L. A. Loevner, A. Mancuso, H. Serrai, D. I. Rosenthal, A. M. Kilger, D. S. Nelson, K. L. Zakian, F. Arias-Mendoza, M. Rijpkema, J. A. Koutcher, T. R. Brown, A. Heerschap and J. D. Glickson: Prediction of treatment response of head and neck cancers with P-31 MR spectroscopy from pretreatment relative phosphomonoester levels. *Acad Radiol*, 9(6), 688-94 (2002)

103. F. Arias-Mendoza, M. R. Smith and T. R. Brown: Predicting treatment response in non-Hodgkin's lymphoma from the pretreatment tumor content of phosphoethanolamine plus phosphocholine. *Acad Radiol*, 11(4), 368-76 (2004)

104. A. Viale, F. Reineri, D. Santelia, E. Cerutti, S. Ellena, R. Gobetto and S. Aime: Hyperpolarized agents for advanced MRI investigations. *Q J Nucl Med Mol Imaging*, 53(6), 604-17 (2009)

105. B. D. Ross, P. Bhattacharya, S. Wagner, T. Tran and N. Sailasuta: Hyperpolarized MR imaging: neurologic applications of hyperpolarized metabolism. *AJNR Am J Neuroradiol*, 31(1), 24-33 (2010)

106. K. Golman, R. I. Zandt, M. Lerche, R. Pehrson and J. H. Ardenkjaer-Larsen: Metabolic imaging by hyperpolarized 13C magnetic resonance imaging for *in vivo* tumor diagnosis. *Cancer Res*, 66(22), 10855-60 (2006)

107. M. J. Albers, R. Bok, A. P. Chen, C. H. Cunningham, M. L. Zierhut, V. Y. Zhang, S. J. Kohler, J. Tropp, R. E. Hurd, Y. F. Yen, S. J. Nelson, D. B. Vigneron and J. Kurhanewicz: Hyperpolarized 13C lactate, pyruvate, and alanine: noninvasive biomarkers for prostate cancer detection and grading. *Cancer Res*, 68(20), 8607-15 (2008)

108. P. E. Larson, R. Bok, A. B. Kerr, M. Lustig, S. Hu, A. P. Chen, S. J. Nelson, J. M. Pauly, J. Kurhanewicz and D. B. Vigneron: Investigation of tumor hyperpolarized [1-13C]-pyruvate dynamics using time-resolved multiband RF excitation echo-planar MRSI. *Magn Reson Med*, 63(3), 582-91 (2010)

109. S. E. Day, M. I. Kettunen, F. A. Gallagher, D. E. Hu, M. Lerche, J. Wolber, K. Golman, J. H. Ardenkjaer-Larsen and K. M. Brindle: Detecting tumor response to treatment using hyperpolarized 13C magnetic resonance imaging and spectroscopy. *Nat Med*, 13(11), 1382-7 (2007)

110. T. H. Witney, M. I. Kettunen, S. E. Day, D. E. Hu, A. A. Neves, F. A. Gallagher, S. M. Fulton and K. M. Brindle: A comparison between radiolabeled fluorodeoxyglucose uptake and hyperpolarized (13)C-labeled pyruvate utilization as methods for detecting tumor response to treatment. *Neoplasia*, 11(6), 574-82, 1 p following 582 (2009)

111. A. L. McKnight, J. L. Kugel, P. J. Rossman, A. Manduca, L. C. Hartmann and R. L. Ehman: MR elastography of breast cancer: preliminary results. *AJR Am J Roentgenol*, 178(6), 1411-7 (2002)

112. M. Bruehlmeier, U. Roelcke, P. A. Schubiger and S. M. Ametamey: Assessment of hypoxia and perfusion in human brain tumors using PET with 18F-fluoromisonidazole and 15O-H2O. *J Nucl Med*, 45(11), 1851-9 (2004)

113. M. Gabriel, C. Decristoforo, D. Kendler, G. Dobrozemsky, D. Heute, C. Uprimny, P. Kovacs, E. Von Guggenberg, R. Bale and I. J. Virgolini: 68Ga-DOTA-Tyr3-octreotide PET in neuroendocrine tumors: comparison with somatostatin receptor scintigraphy and CT. *J Nucl Med*, 48(4), 508-18 (2007)

114. A. J. Beer, M. Niemeyer, J. Carlsen, M. Sarbia, J. Nahrig, P. Watzlowik, H. J. Wester, N. Harbeck and M. Schwaiger: Patterns of alphavbeta3 expression in primary and metastatic human breast cancer as shown by 18F-Galacto-RGD PET. *J Nucl Med*, 49(2), 255-9 (2008)

Key Words: Cancer, functional imaging, molecular imaging, PET, MRI, CT, Review

Send correspondence to: Drew A. Torigian, Department of Radiology, Hospital of the University of Pennsylvania, 3400 Spruce Street, Philadelphia, PA 19104, Tel: 215-615-3805, Fax: 215-614-0033, E-mail: Drew.Torigian@uphs.upenn.edu

http://www.bioscience.org/current/vol4E.htm